An expansion-coalescence model for bubble growth in viscous fluids

Alain Burgisser, Louis Forestier-Coste, François James, Simona Mancini

An expansion-coalescence model for bubble growth in viscous fluids*

A. Burgisser[a], L. Forestier-Coste[b], F. James[c], S. Mancini[c]

a *Institut des Sciences de la Terre, CNRS - IRD - Université de Savoie, Campus Scientifique, 73376 Le Bourget du Lac Cedex, France.*

b *Université de Bordeaux, IMB, UMR 5251, F-33400 Talence, France.*

c *Université d'Orléans, Fédération Denis Poisson, FR CNRS 2964, MAPMO, UMR CNRS 7349, Route de Chartres, BP. 6759, 45067 Orléans Cedex 2, France.*

AMS Classification: 82C22, 35Q90, 65C20

Abstract

We statistically describe at a mesoscopic level the growth by decompression, exsolution and coalescence of a population of gas bubbles immersed in a viscous fluid. The model treats in particular the case of water gas bubbles entrained in a viscous magma ascending in a volcano conduit. Bubbles are characterized both by their volume and mass, but are homogeneously distributed in space and have no relative velocity. Volume and mass growth rates as well as the coalescence operator are defined starting from a microscopic model and by means of physical arguments. Numerical simulations show a good agreement of the computed volumes distributions with those measured in experiments, justifying the importance to consider coalescence in this framework and the need of more precise experiences in order to better validate the coalescence kernel.

*This work was partially founded by the ERC-starting grant DEMONS (n. 202844) under the European FP7.

1 Introduction

Volcanic eruptions are classified in two families: effusive and explosive. The first ones are characterized by the separate emission of magma and gas. The resulting lava flows or lava domes affect the immediate neighborhood of the volcano. The second ones are more dangerous and are characterized by columns of cinders which may measure several kilometers. When falling on the ground these cinders may accumulate and break human infrastructures as well as pollute air. Finally, both eruptions may lead to pyroclastic avalanches that sweep the volcano flanks at high speeds and cause devastation up to dozens of kilometers from the source. Thus, the understanding of the mechanisms driving volcanic eruptions is useful for both scientific and societal reasons.

It is nowadays clear that the evolution of gas bubbles in very viscous magmas such as rhyolite affect the kind of eruption the volcano may have. This is why we are interested in the modeling of bubbles growth in viscous magmas during an eruption.

While ascending to the surface through volcano conduits, bubbles growth in viscous magmas is governed by decompression and exsolution of volatiles (mainly water) from the magma surrounding the bubbles to the bubbles. This phenomena is usually modeled considering that bubbles are mono-dispersed, i.e. they all evolve in the same way and have the same initial radius (or volume) and mass (or pressure). The most commonly used model consists of a system of two ordinary differential equations describing the time evolution of the radius and mass of a single bubble and coupled with an advection-diffusion equation modeling the space-time evolution of the volatile concentration in the magma surrounding the bubble, see for example [14], [11] and [4]. Two previous works, [9] and [11], analyzed the dimensionless associated system of equations. This is characterized by two relaxation parameters, namely Θ_V and Θ_D, which vary by several order of magnitude and account for viscous ($\Theta_D \ll \Theta_V$), diffusive ($\Theta_V \ll \Theta_D$) or equilibrium ($\Theta_V \sim \Theta_D$) growth regimes. In particular, in the diffusion regime, for $\Theta_V \ll 1$, the magma-bubble system is at the mechanical equilibrium; in the viscous regime, for $\Theta_D \ll 1$, the magma-bubble system is at the chemical equilibrium; finally, in the equilibrium regime, for $\Theta_V, \Theta_D \ll 1$, the magma-bubble system is at the thermodynamical equilibrium. In [9] we numerically show that when both relaxation parameters converges to zero computational times are very long, and we propose some simplified models of the system to be used for these extremes values of Θ_V and Θ_D.

Although this mono-disperse bubbles population model gives very good results,

as far as porosity is concerned with, when compared to experimental data (see [9] and [13]), it assumes that bubbles are isolated, not taking into account their interaction, i.e. the coalescence of two (or more) bubbles. Leaving aside coalescence is a severe limitation because of its large impact on the size distribution and because coalescence can create an interconnected network of bubbles from which the gas can escape from magma. Such gas run away is a main control on whether an eruption is effusive or explosive. There have been attempts to overcome the absence of coalescence in models. For instance, in [12] is presented a kinetic model describing the evolution of the distribution function of a set of bubbles that grow by decompression and coalescence. The distribution function $f = f(t, v)$ represents in [12] the probability to find at time t a bubble of volume v, and the model is homogeneous in space. The volume growth rate is defined by an exponential function, corresponding to a growth at the thermodynamical equilibrium. The bubbles coalescence is described by a Smoluchowski type operator. Up to our knowledge, this is the only work presenting a statistical description of poly-disperse bubble growth in magma. Nevertheless, this model cannot describe the evolution of a bubble population when considering non-equilibrium growth, as for example growth of bubbles at the chemical equilibrium and not at the mechanical one, $\Theta_V \gg \Theta_D \to 0$.

Therefore our aim is to propose a more general kinetic model describing the evolution of bubbles populations also for non-equilibrium growths. The abstract writing of the kinetic model is rather classic by means of Liouville theorem. The main goal is to define coalescence operator and rate depending on the volume and mass variables and not on position and velocity, as usual, and to validate it on a set of experimental data. Our coalescence operator turns out to be two-dimensional and is in some sense a direct generalization of the Lovejoy model [12]. Due to their complexity, two-dimensional coalescence operators have been rarely studied and simulated in the past, see for example [16] and [10]. In [8], a numerical scheme is developed and validated by several numerical tests for the two-dimensional continuous Smoluchovski equation. We point out that in our modeling we have to overpass one main difficulty: to simplify the system of equations of the mono-disperse model in order to avoid the coupling with the advection-diffusion equation, so to diminish computational costs.

This paper is organized as follows. In section 2 we present the abstract kinetic model and recall the main properties of its solution. Volume and mass rates are described in section 3, while section 4 is devoted to coalescence kernels. Next, in section 5 we describe the numerical discretization of the model. Finally, numerical results, together with their comparison with experimental data are gathered in sec-

tion 6. In section 7 we discuss the proposed model and results and present some research directions to be further investigated.

2 The kinetic model

We want to describe at a statistical level the evolution of gas bubbles by decompression, exsolution and coalescence in a very viscous fluid. In this section we introduce the kinetic equation we will use to model this phenomena and recall the main properties of its solution.

We note that our kinetic model is defined on non-standard independent variables, since there is no dependence on bubbles velocity and position. In fact, we assume that bubbles are entrained by the magma which raises in the conduit with a laminar and constant velocity u, see also [12]. This is a first approximation since of course the magma fluid satisfies the Navier-Stokes equations for an incompressible fluid. By this assumption it follows that bubble positions are only related here to their depth in the conduit (and not to their distance from the conduit borders), which in his turn is linked to the magma pressure. Hence bubble positions are implicitly defined by the value of the magma pressure. This is consistent with experimental data which are obtained considering small samples of magma, where bubbles are homogeneously distributed in space and where their displacements can be neglected.

Therefore the distribution function $f = f(t, v, m)$ represents the probability to find at time $t \geq 0$ a bubble of volume $v \in [v_{min}, \infty]$ and mass $m \in [m_{min}, \infty]$. In the following, we will then consider the domains

$$\Omega_T = [0, T] \times \Omega, \text{ and } \quad \Omega = [v_{min}, \infty] \times [m_{min}, \infty],$$

describing the time interval and the phase space in which the bubbles evolution takes place, and, for brevity, we will denote by ω the phase space variables (v, m), we shall call ω the size of a bubble, implicitly meaning the bubble volume and mass; $d\omega$ will denote the infinitesimal element $dv\, dm$. This choice of variable is consistent with the mono-disperse model described in [11].

Since bubbles grow by expansion and coalescence, the distribution function $f(t, v, m)$ must satisfy the following kind of kinetic equation:

$$\partial_t f + \partial_v(V f) + \partial_m(M f) = Q(f). \tag{1}$$

The left-hand side in (1) is a conservative equation and describes the evolution by decompression and exsolution of the set of bubbles, where the two growth rates for

the volumes and masses are defined by the non-linear functions $V = V(t, v, m)$ and $M = M(t, v, m)$, respectively:

$$V(t, v, m) = \frac{3}{\Theta_V}(m - \overline{V}), \tag{2}$$

$$M(t, v, m) = \frac{1}{\Theta_D}(\overline{M} - m), \tag{3}$$

with $\overline{V} = \overline{V}(t, v)$ and $\overline{M} = \overline{M}(t, v)$ two equilibrium manifolds. Their expression will be given when introducing the volcanology model, see section 3. We note here that this kind of rates implies incoming drift on the boundaries.

The right-hand side in (1) describes bubbles coalescence by means of the Smoluchowski continuous coalescence operator:

$$\begin{aligned} Q(f)(t, v, m) = \frac{1}{2}\int_0^{\omega} H(t, \omega', \omega - \omega')\ f(t, \omega')\ f(t, \omega - \omega')\ d\omega' \\ - f(t, \omega)\int_0^{\infty} H(t, \omega', \omega)\ f(t, \omega')\ d\omega', \end{aligned} \tag{4}$$

where the integrals have to be understood in the two-dimensional setting (v, m). Moreover, $H(t, \omega, \omega')$ is the coalescence kernel which must be positive and symmetric,

$$H(t, \omega, \omega') > 0\ , \quad H(t, \omega, \omega') = H(t, \omega', \omega).$$

Its expression will be given later on, see section 4. We recall here that the first term on the right-hand-side of (4) is the gain term and counts the bubbles created by the coalescence of a bubble of size ω' and one of size $\omega - \omega'$. The second term on the right-hand-side of (4) is the loss term and counts the bubbles of size ω disappearing by coalescence with all other bubbles.

To conclude the description of the coalescence phenomena, we must describe how the sizes of two coalescing gas bubbles define the size of the created single bubble. Let us denote by (v', m') and (v'', m'') the sizes of the two coalescing bubbles and by (v, m) the size of the created one. It is physically natural to assume that masses sum up, but this is not the case for volumes. We recall that we have a poly-disperse population of bubbles and that in our model volume and mass are independent variables. This is rather different with respect to the modeling usually done when considering polymers, in which mass and volume are equivalent, see for example [5] or [2] and references therein. Nevertheless, we have no way to know how volumes

combine for two gas coalescing bubbles and therefore, in a first approach, we shall assume here that they do actually sum up. In conclusion volumes and masses verify:

$$v = v' + v'' , \quad m = m' + m'' ,$$

and, as a consequence of the perfect gas law holding in each bubble, the pressure p in the created bubble may be given as a convex combination of the pressures in the two coalescing bubbles p' and p'':

$$p = \delta p' + (1 - \delta) p'' , \quad \delta = \frac{v'}{v' + v''}.$$

We associate to (1) an initial condition $f_0 = f_0(v, m) \geq 0$ describing the distribution of bubbles at the initial time 0 in the phase-space Ω. The initial condition f_0 given by the experimental measures, is defined by a sum of Dirac masses. Concerning the boundary conditions, we assume that there do not exist bubbles with volume or mass equal to zero :

$$f(t, 0, m) = f(t, v, 0) = 0,$$

and that for large values of v or m the distribution function f decays to zero :

$$\lim_{v \to \infty} f(t, v, m) = \lim_{m \to \infty} f(t, v, m) = 0.$$

The numerical phase space domain will be bounded both in v an m, and we will then consider no flux conditions for the larger values of v and m. On the other hand for $v = 0$ or $m = 0$ we note that the respective drifts are coming into the domain (see (2) and (3)), so that if the initial condition $f_0 = 0$ for $v = 0$ or $m = 0$ are set (which seems natural), then $f = 0$ at each time.

Let us recall now some mathematical properties of the expansion-coalescence equation (1). Let r and s be two integers, then the moments $\mathcal{M}_{r,s} = \mathcal{M}_{r,s}(t)$ of order $p = r + s$ of the distribution function f are given by:

$$\mathcal{M}_{r,s} = \int_0^\infty v^r \, m^s \, f(t, \omega) \, d\omega \ . \tag{5}$$

For instance, the zero order moment:

$$\mathcal{M}_{0,0} = \int_0^\infty f(t, v, m) \, dv \, dm \ , \tag{6}$$

represents the number of bubbles $\mathcal{N}(t) = \mathcal{M}_{0,0}$; the first order moment (for $r = 1$ and $s = 0$):

$$\mathcal{M}_{1,0} = \int_0^\infty v\, n(t, v, m)\; dv\, dm\ , \tag{7}$$

represents the volume occupied by the bubbles, $\mathcal{V}(t) = \mathcal{M}_{1,0}$; and the first order moment (for $r = 0$ and $s = 1$):

$$\mathcal{M}_{0,1} = \int_0^\infty m\, n(t, v, m)\; dv\, dm\ , \tag{8}$$

represents the mass of the bubbles, $\mathcal{M}(t) = \mathcal{M}_{0,1}$.

Since the left-hand side of equation (1) is a conservation equation, when neglecting coalescence, the number of bubbles must be conserved, that is $\mathcal{N}(t) = \mathcal{N}(0)$. This can be proved integrating over the interval $[0, t]$. On the other hand, when neglecting the expansion terms in (1), the first order moments, $\mathcal{M}_{1,0}$ and $\mathcal{M}_{0,1}$, must be conserved at least until the gelation time, if any, is reached, see [6], [8] and reference therein. This means that the bubbles volume and the bubbles mass must be conserved : $\mathcal{V}(t) = \mathcal{V}(0)$ and $\mathcal{M}(t) = \mathcal{M}(0)$. We finally remark that if the first order moments are constant in time, then any linear combination of them will be constant in time, too. We note here that at a discrete level it will not be possible to conserve both first order moments and we will then choose to conserve only the bubbles mass, see [8].

3 Growth rates

In order to define the volume and mass growth rates, we have to come back to the microscopic, or mono-disperse, model. We recall here the coupled system of equations governing the growth of a single bubble as it is presented in its dimensionless form in [11].

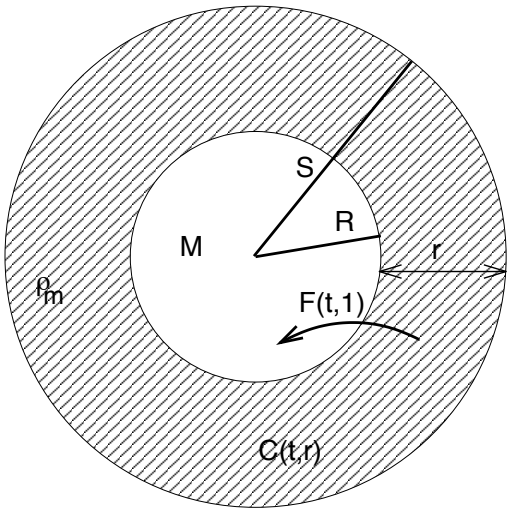

Figure 1: A single bubble (white) with its surrounding influence region (hatched). The function $F(t,1)$ is the volatile flux incoming the bubble from the influence region, ρ_m is the magma density, R, S, M and $C(t,r)$ respectively are the radii of the bubble and of the influence region, the bubble mass and the volatile concentration in the influence region.

Assuming that a bubble is surrounded by an influence domain (that is the region of magma exchanging gas with the bubble) represented by a sphere of radius S, see figure 1, the radius R and mass M of a volatile bubble growing in a viscous magma by decompression and exsolution are governed by the following system of two ordinary differential equations:

$$\dot{R} = \frac{R}{\eta_{eff}\Theta_V}\left(P - P_a(t) - \frac{\Sigma}{R}\right), \tag{9}$$

$$\dot{M} = \frac{3\rho_m}{\Theta_D}F(t,R), \tag{10}$$

where η_{eff} is the magma viscosity, ρ_m the magma density, Σ the surface tension between the gas and the magma, $P_a(t)$ the ambient (magma) pressure which will be detailed later on, and Θ_V and Θ_D are two relaxation parameters accounting for viscosity and diffusion, see section 6 for more details.

Equation (9) states that the time evolution of a bubble radius is governed by the difference between the bubble pressure and the magma pressure augmented by the surface tension.

Equation (10) is the differential version of the conservation of mass, which states that the variation of the bubble mass is equal to the mass of volatile diffusing between the magma and the bubble.
In (10) the flux $F(t, R)$ is defined by means of the volatile concentration in the magma surrounding the bubble, $C = C(r, t)$, satisfying the following advection-diffusion equation, for $t > 0$ and $r \in [R, S]$:

$$\partial_t C + \frac{R^2 \dot{R}}{r^2} \partial_r C = \frac{1}{\Theta_D} \frac{1}{r^2} \partial_r \left(r^2 D \partial_r C \right), \tag{11}$$

with D the diffusion coefficient and the following boundary conditions:

$$C(t, R) = C_H \sqrt{P}, \quad (r^2 D \partial_r C)_{r=S} = 0, \tag{12}$$

In equation (11), the left-hand side is an advective term that takes into account the fact that the border of the bubble moves with a radial velocity given by $\dot{R}R^2/r^2$, thanks to the incompressibility of the magma. The right-hand side describes the radial diffusion of the volatile.

The left boundary condition in (12) asserts that the bubble boundary and the magma are at a chemical equilibrium, which is described by the solubility condition, with $C_H = K_H \sqrt{P_i}$, P_i the initial pressure and K_H the Henry solubility constant. The right boundary condition in (12), states that at the outer border ($r = S$) of the influence region the concentration flux is null, i.e. there is no volatile loss or gain. Finally, the initial concentration is assumed to be homogeneous in space $C(0, r) = C_i$, which is equal to C_H if the initial state is at the chemical equilibrium.

The incoming volatile flux in the bubble $F(t, R)$ is then defined by:

$$F(t, R) = \left(r^2 D \partial_r C \right)_{r=R}. \tag{13}$$

Following [11], assuming that the magma raises at a constant velocity, implies that magma pressure is linearly decreasing. The magma pressure eventually reaches a final value, which is the pressure at the surface of the volcanic conduit normalized to 0. The fact that pressure cannot become negative implies that time t belongs to the bounded interval $[0, 1]$. Hence, we assume that the ambient pressure $P_a(t)$ satisfies in dimensionless form:

$$P_a(t) = 1 - t. \tag{14}$$

Therefore, we may consider the magma pressure as a dimensionless time, recovering information on the depth of the bubbles in the conduit.

Following [11], the volume of the influence region $S^3(t)$ is constant in time so that it satisfies:

$$S^3 = R^3 + S_0^3, \tag{15}$$

with S_0^3 the dimensionless volume occupied by the magma surrounding a bubble of radius zero, see figure 1.

We note that (9) can be written in the form

$$\dot{R} = \frac{R}{\Theta_V}(P - \overline{P}), \tag{16}$$

where the equilibrium manifold $\overline{P} = \overline{P}(t, R)$ is given by:

$$\overline{P}(t, R) = P_a(t) + \frac{\Sigma}{R}, \tag{17}$$

which is the mechanical equilibrium $\Theta_V \to 0$.

In order to diminish computational costs we want to avoid the coupling with the advection-diffusion equation (11) in (10). By analogy with the radius growth, we introduce the equilibrium manifold defined by the chemical equilibrium case, that is when $\Theta_D \to 0$:

$$\overline{M} = \overline{M}(R) = \frac{\left(-YC_H + \sqrt{Y^2C_H^2 + 4R^3YC_0}\right)^2}{4R^3}, \tag{18}$$

with $Y = \rho_m S_0^3$, C_0 the total volatile concentration when the bubble radius is zero, and A a scaling function. We replace (10) by:

$$\dot{M} = \frac{A}{\Theta_D}(\overline{M} - m). \tag{19}$$

Numerical comparisons show that the choice $A = 1$ is relevant. The accuracy, for different values of the relaxation parameters, of this simplification is shown in section 6.

We finally note that the macroscopic quantities measured in experiments are the bubble radius R (or their volume V) and the porosity $\alpha = \alpha(t)$, that is the fraction of volume occupied by the volatile with respect to the total volume. In the case of a single bubble surrounded by its influence region, the porosity may be computed by the following formula, see [11]:

$$\alpha(t) = \left(\frac{R}{S}\right)^3. \tag{20}$$

When considering a population of bubbles, under the assumption that the volume of magma is constant, see (15), we can compute the porosity by:

$$\alpha(t) = \frac{\mathcal{V}}{\mathcal{V} + \mathcal{W}_0} \, , \tag{21}$$

where $\mathcal{V} = \mathcal{V}(t)$ is the volume of bubbles defined by $\mathcal{V} = \mathcal{M}_{1,0}$, see (7), and $\mathcal{W}_0$ is the magma volume. Knowing the initial porosity α_0 and the initial distribution $f_0 = f(0, v, m)$, we can determine $\mathcal{W}_0$ using (21):

$$\mathcal{W}_0 = \frac{1 - \alpha_0}{\alpha_0} \, \mathcal{V}_0. \tag{22}$$

We note that, since the first order moment is conserved by the coalescence operator, the only variation for the porosity will be given by the left-hand side of equation (1), and so the numerical results for porosity obtained by means of the mono-disperse model and the one obtained by means of the kinetic equation must be identical, unless gelation occurs.

4 Coalescence kernel

We now consider the coalescence of two bubbles of sizes $\omega' = (v', m')$ and $\omega'' = (v'', m'')$ that yields to a single bubble of size $\omega = (v, m)$. We assume that the coalescence is instantaneous and that the relaxation time of the created bubble to get back to a spherical geometry is zero. Hence, we neglect the possibility of having a chain of coalescing bubbles, although this is an important and observed behavior, see [1]. Bubble chains influence the way volatiles may escape from magma and is thus linked to the type of eruption the volcano has. Multiple coalescence and bubble chains may be studied in future works by considering for instance a new characteristic for the bubble population linked to the geometrical form of the created bubble.

We recall that bubbles have no relative velocity, hence the only way they may coalesce is by expanding until the film of magma in between two bubbles is too thin to hold and breaks up. We want to define a physical relevant coalescence kernel $H = H(t, \omega, \omega')$ which is positive and symmetric. The coalescence kernel represents the rate of coalescence and it has the dimension of the inverse of a time. Under the assumption that the mass of the magma film contained in between the walls of two coalescing bubbles is conserved during the coalescence process, in [3] are described and compared two coalescing times : the planar profile one, $\mathcal{T}_p$, and the stretch one, $\mathcal{T}_s$. The coalescence kernel is then defined by:

$$H_p(t, \omega, \omega') = 1/\mathcal{T}_p \, , \qquad H_s(t, \omega, \omega') = 1/\mathcal{T}_s.$$

In figure 2 we show the two configurations of coalescing bubbles, on the left the planar coalescence and on the right the stretch one, in gray the region in which magma mass is conserved.

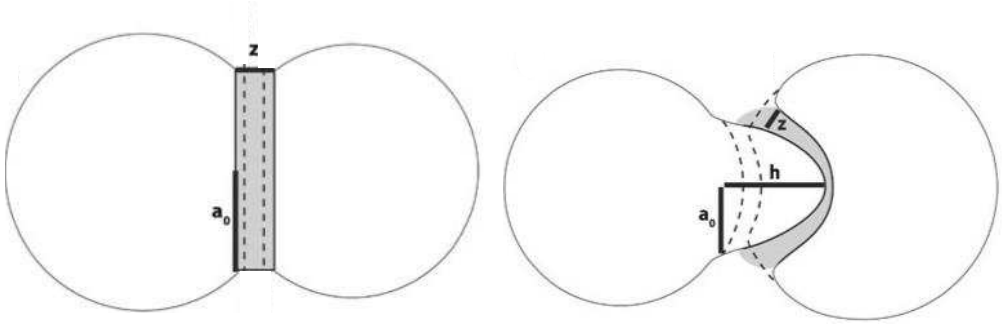

Figure 2: Two coalescing bubbles : planar (left) and stretch (right) profiles.

We detail here the computations leading to the definition of the planar coalescence kernel $H_p(t, \omega, \omega')$. For the discussion in the case of the stretching kernel (or time) we refer the reader to [3]. The magma film mass contained in the flat plane between two merging bubbles is given by:

$$m_m(t) = \rho_m \pi z(t) a^2(t),$$

where $z(t)$ is the distance between the bubbles and $a(t)$ corresponds to the radius of the disc of the flat section of the bubble (which is assumed to be the same for each bubble), see Figure 2. Assuming that $m_m(t)$ is constant in time it is possible to define a rate of coalescence $H_p(t, \omega', \omega'')$ of two merging bubbles, which border approach with a speed c, as the inverse of the time needed to reach the breaking film distance, z_f, see [3].

$$H_p(t, \omega, \omega') = \frac{c}{a_0} \left(\frac{\sqrt{z_f}}{\sqrt{z} - \sqrt{z_f}} \right).$$

For instance, we assume that $a(t)$ linearly grows in time, $a(t) = a_0 + ct$, with a_0 the initial radius given by

$$a_0 = \varepsilon((v')^{1/3} + (v'')^{1/3})/2, \tag{23}$$

with $0 < \varepsilon \ll 1$, and c the rate at which the film thin-off, which is given here by the mean between the two bubbles radius growth rates,

$$c = (\dot{R}' + \dot{R}'')/2.$$

The factor ε and the final distance z_f (before break out) are determined by the physical characteristics of the magma and by experimental measures. We finally obtain the following coalescence kernel:

$$H_p(t,\omega',\omega'') = \frac{(\dot{R}'+\dot{R}'')_+}{\varepsilon((v')^{1/3}+(v'')^{1/3})}\frac{\sqrt{z_f}}{(\sqrt{z}-\sqrt{z_f})_+}\ , \tag{24}$$

where the distance between the two bubbles $z = z(t)$ may be expressed in terms of the volume of each bubble and of the porosity α of the magma:

$$z = \left((v')^{1/3}+(v'')^{1/3}\right)\left(\frac{1-\alpha^{1/3}}{\alpha^{1/3}}\right). \tag{25}$$

This kernel is positive and symmetric. Considering the homogeneous coalescence equation $\partial_t f = Q_p(f)$, with the kernel defined by (24) and (25), we have the following:

Proposition 4.1 *For any function $g(v,m)$, the functions $f_s = f_s(v,m)$ given by*

$$f_s(m,v) = \begin{cases} 0 & \text{if } m > \Sigma v^{2/3}, \\ g(m,v) & \text{otherwise,} \end{cases} \tag{26}$$

are equilibrium states of the coalescence operator $Q_p(f_s)$.

Proof: We first note that if $f = f(t,\omega)$ is a non-trivial solution, that is if $f \neq 0$ and $Q_p(f) = 0$ then we also have

$$\int_0^\infty Q_p(f)\ d\omega'' = 0,$$

which is equivalent to

$$-\frac{1}{2}\int_0^\infty\int_0^\infty H_p(t,\omega',\omega'')\, f(t,\omega')\, f(t,\omega'')\ d\omega'\ d\omega'' = 0. \tag{27}$$

We seek for non-trivial solutions, thus (27) holds if and only if $H_p(t,\omega',\omega'') = 0$, that is if and only if $(\dot{R}'+\dot{R}'')_+ = 0$.
Let us define the function $k(t)$ for $t \in [0,1]$ as

$$\begin{aligned} k(t) &= \Theta_V(\dot{R}'+\dot{R}'') \\ &= \frac{m'}{(v')^{2/3}} - (1-t)(v')^{1/3} - \Sigma + \frac{m''}{(v'')^{2/3}} - (1-t)(v'')^{1/3} - \Sigma \\ &= t((v')^{1/3}+(v'')^{1/3}) - ((v')^{1/3}+(v'')^{1/3}) + \frac{m'}{(v')^{2/3}} + \frac{m''}{(v'')^{2/3}} - 2\Sigma. \end{aligned}$$

Note that $H_p(t,\omega',\omega'')=0$ if and only if $k\leq 0$. Since $k(t)$ is increasing in time, if $k(1)\leq 0$ then $k(t)\leq 0$ and $H_p(t,\omega',\omega'')=0$ for all $t\in[0,1]$. It is easily seen that $k(1)$ is negative if

$$\frac{m'}{(v')^{2/3}}+\frac{m''}{(v'')^{2/3}}\leq 2\Sigma. \tag{28}$$

Assume that (m',v') and (m'',v'') verify (28) so that $\dot{R}'+\dot{R}''<0$. We have to consider two possibilities.
i) The first one is $m'>\Sigma(v')^{2/3}$ and $m''<\Sigma(v'')^{2/3}$, then the growth rates are such that $\dot{R}'>0$ and $\dot{R}''<0$. However, $H_p(1,\omega',\omega')>0$, and $f(t,\omega')$ must be the zero function for this choice. In other words if one of the two growth rate is positive, the stationary solution must be the trivial one.
ii) The second possibility is $m'<\Sigma(v')^{2/3}$ and $m''<\Sigma(v'')^{2/3}$, Then $\dot{R}'<0$ and $\dot{R}''<0$, so that $H_p(t,\omega',\omega'')=0$. Moreover, $H_p(t,\omega,\omega)=0$, so that $f(t,\omega)$ may be non-zero for all time t. In other words, there is a non-trivial stationary solution.
This can be resumed by defining the steady state $f_s(\omega)$ by (26).
On the contrary, it is clear that $\partial_t f_s=0$ and replacing f_s in (27), we also obtain that $Q_p(f_s)=0$. ∎

From a physical point of view, Proposition 4.1 means that if both bubbles have negative radius growth rates, that is if $m<\Sigma v^{2/3}$ for both bubbles, then they cannot coalesce.

Concerning the stretching coalescence kernel, following [3], we can define $H_s(t,\omega,\omega')$ as, see [3] for more details:

$$H_s(t,\omega,\omega')=\frac{z}{2a_0|P'-P''|},$$

where a_0 and z are defined as for the planar kernel, (23) and (25), and $|P'-P''|$ is the difference of pressure between the two merging bubbles and can be computed knowing the volume and mass of each bubble, by means of the perfect gas law $P=m/v$:

$$H_s(t,\omega,\omega')=\frac{v'\ v''}{\epsilon|v''\ m'-v'\ m''|}\left(\frac{1-\alpha^{1/3}}{\alpha^{1/3}}\right) \tag{29}$$

From the expression (29) we see that, on the contrary of what happens for Q_p, there is no equilibrium state for Q_s, and that the coalescence kernel H_s can be defined only for bubbles having different gas pressures.

5 Numerical resolution

In the previous sections we have introduced all the ingredients needed to build the kinetic model. We resume here the complete model and the first step is to write the preceding equations in terms of mass and volume. The expansion-coalescence of a population of bubbles is governed by the kinetic equation (1):

$$\partial_t f + \partial_v(V f) + \partial_m(M f) = Q(f),$$

where the density function $f = f(t, v, m)$ represents the distribution of bubbles at time t in terms of their volumes v and masses m. We underline once more that this model is based on the non-standard variables volume v and mass m, and has no kinetic variable as position x or velocity v. The respective expansion rates V and M are defined by (2) and (3):

$$V(t, v, m) = \frac{3}{\Theta_V}\left(m - (1-t)v - \Sigma v^{2/3}\right), \tag{30}$$

$$M(t, v, m) = \frac{1}{\Theta_D}\left(\frac{\left(-C_H\rho_m w + \sqrt{C_H^2\rho_m^2 w^2 + 4\rho_m v w C_0}\right)^2}{4v} - m\right), \tag{31}$$

where w is the volume of the influence region defined in analogy to (22):

$$w = \frac{1-\alpha}{\alpha}\, v\,, \tag{32}$$

and where the coalescence operator takes the form of the Smoluchowski continuous coalescence operator (4), with the kernel given by expression (24) or (29).

By defining the influence region volume w by (32), we have reduced the number of variables for the distribution function. In fact, by considering relation (15) we should take into account $f = f(t, v, m, w)$ with a zero growth rate in terms of the variable w. From a physical point of view, definition (32) says that bubbles occupying the same volume v have the same influence region w. This assumption may be relaxed, but this has computational costs, since the numerical resolution would involve three variables.

We turn now to the discretization of the model. We split the numerical resolution of (1) in two parts. At each time step we first solve explicitly in time the coalescence term, right-hand-side of (1), and then implicitly in time the expansion term, left-hand-side of (1). We note that this is equivalent to solve the whole equation (1) in a

single time step. In fact, for $n \in \mathbb{N}$, let us denote the discrete times by t^n, the time steps by $\Delta t^n = t^{n+1} - t^n$ and the time discretization of the distribution function by $f^n = f(t^n, v, m)$. Then the explicit discretization of the coalescence step reads:

$$\tilde{f}^{n+1} = f^n + \Delta t^n \zeta(t^n) Q(f^n),$$

where $\tilde{f}^{n+1}$ denotes the value of the numerical solution after the coalescence step and has to be used to compute the expansion term. Then, the implicit discretization of the expansion term is given by:

$$f^{n+1} + \Delta t^n \left(\partial_v (V^{n+1} f^{n+1}) + \partial_m (M^{n+1} f^{n+1}) \right) = \tilde{f}^{n+1}.$$

Combining the two discretizations we obtain:

$$\frac{f^{n+1} - f^n}{\Delta t^n} + \partial_v (V^{n+1} f^{n+1}) + \partial_m (M^{n+1} f^{n+1}) = \Delta t^n \zeta(t^n) Q(f^n),$$

which is a semi-implicit time discretization of (1).

We will not detail here the discretization of the coalescence term. This has been the subject of [8], where a multi-dimensional numerical scheme is studied, defined on non-uniform meshes and such that the first order moment is conserved. We note that, in the multi-dimensional framework, it must be chosen which first moment to conserve, since numerically it is not possible to conserve simultaneously all the first moments. We choose to conserve the moment representing the total mass of water $\mathcal{M}(t) = \mathcal{M}_{0,1}(t)$. We finally recall that this model is among the firsts considering two-dimensional coalescence and that numerical schemes for this kind of problem have not been widely studied yet, see [15], [16], [17].

The scheme solving the expansion term is implicit in time because we want to avoid a stability (CFL) condition for this time discretization. Indeed, solving explicitly the expansion term would imply a CFL condition on the time step Δt^n, which is bounded by the minimum of the relaxation parameters Θ_V and Θ_D. This causes very long computational times, in particular when considering the chemical and/or mechanical equilibrium ($\Theta_V \ll 1$ and/or $\Theta_D \ll 1$). By using an implicit scheme, the time step will be fixed by the positivity condition on the coalescence term which is only bounded by the Θ_V parameter, see [8].

The experimental measurements are usually defined on a uniform mesh in terms of the bubbles radii, conditioning the discretization in v and m. This distribution of initial radii will be chosen as the basis to write the grid mesh in volume and mass,

assuming that measurements are done at the thermodynamical equilibrium. Hence, fixing N grid points, we have for $i = 1 \dots N$, the following definitions for the mesh points in v and m:

$$v_{i-1/2} = \left(\frac{R_0 + i\Delta R}{R_i} \right)^3 , \quad m_{i-1/2} = v_{i-1/2} + \Sigma v_{i-1/2}^{2/3} ,$$

where R_i is the mean radius of the initial data (used also for the scaling), R_0 is the minimum radius considered in experiments and ΔR is the step of the uniform grid defining the initial data. We also define the space mesh sizes:

$$\Delta v_i = v_{i+1/2} - v_{i-1/2} , \quad \Delta m_i = m_{i+1/2} - m_{i-1/2} ,$$

and the middle grid points:

$$v_i = (v_{i+1/2} + v_{i-1/2})/2 , \quad m_i = (m_{i+1/2} + m_{i-1/2})/2 .$$

For $n \in \mathbb{N}$ and $i, j = 1 \dots N$, we can now define the discrete distribution function f_{ij}^n which is an approximation of $f(t^n, v_i, m_j)$, and the discrete marginal with respect to the volume:

$$\mathcal{V}(v_i) = \sum_{j=1}^{N} f_{ij}^n \Delta m_j .$$

We split the numerical resolution of the expansion part in two steps: first we consider the discretization implicit in time of the term $\partial_v(Vf)$, then we solve the part concerning $\partial_m(Mf)$. This is equivalent to a directional splitting, solving first equation:

$$\partial_t f + \partial_v(Vf) = 0, \tag{33}$$

and then equation:

$$\partial_t f + \partial_m(Mf) = 0. \tag{34}$$

We report here the implicit finite difference scheme for (33), equation (34) being solved analogously. Let j be fixed and $i = 1 \dots N$, and define:

$$V_{ij}^n = \frac{3}{\Theta_V} \left(m_j - v_i(1 - t^n) - \Sigma v_i^{2/3} \right)$$

and its positive and negative parts:

$$\left(V^+\right)_{ij}^n = \max(0, V_{ij}^n) , \quad \left(V^-\right)_{ij}^n = \min(0, -V_{ij}^n) .$$

Then the equation (33) is discretized implicitly in time by:

$$\left(1+\frac{\Delta t}{\Delta v_i}|v_{ij}^{n+1}|\right) f_{ij}^{n+1} - \frac{\Delta t}{\Delta v_i}\left((V^+f)_{i-1,j}^{n+1} + (V^-f)_{i+1,j}^{n+1}\right) = f_{ij}^n \tag{35}$$

To solve this implicit bi-dimensional scheme we transform it by writing the unknown square matrix f_{ij}^n of size $N \times N$, in a vector X_h^n of size N^2: for each time step n and index $j = 1 \dots N$ we define $h = i + (j-1)N$ for $i = 0 \dots N$ and $X_h^n = f_{i,j}^n$, that is:

$$X^n = (f_{1,1}^n, f_{2,1}^n, f_{3,1}^n, \dots, f_{N-2,N}^n, f_{N-1,N}^n, f_{N,N}^n)^T.$$

Moreover, we define the vectors a^n, c^n of size $N^2 - 1$ by, for $j = 1 \dots N$:

$$a_h^n = \begin{cases} -\frac{\Delta t}{\Delta v_i}(V^-)_{i+1,j}^n\,, & i = 1 \dots N-1 \\ 0\,, & i = N \end{cases}$$

$$c_h^n = \begin{cases} -\frac{\Delta t}{\Delta v_i}(V^+)_{i-1,j}^n\,, & i = 2 \dots N \\ 0\,, & i = 1 \end{cases}$$

and the vector b^n of size N^2 by, for $i, j = 1 \dots N$:

$$b_h^n = 1 + \frac{\Delta t}{\Delta v_i}|V_{ij}^n|\,,$$

and the tridiagonal matrix D^n which the h^{th} line reads:

$$D_h^n = (0 \dots 0\ c_h^n\ b_h^n\ a_h^n\ 0 \dots 0).$$

The discrete equation (35) then reads:

$$D_{h,h-1}^{n+1} X_{h-1}^{n+1} + D_{h,h}^{n+1} X_h^{n+1} + D_{h,h+1}^{n+1} X_{h+1}^{n+1} = X_h^n\,, \tag{36}$$

which is solved by a LU decomposition.

We can solve in the same way the equation (34). The algorithm involves, for the expansion term, at each time step n the resolution of (33) and then (34), before returning the resolution of the coalescence part.

6 Numerical and experimental results

We briefly explain how experiments are done because our numerical simulations are compared with experimental data, see [1]. Various samples of the same magma

are placed with water in sealed capsules and heated under high pressure for several days in order to ensure water saturation. A sudden decompression step at constant temperature, nucleates bubbles, that is creates microscopic gas bubbles (the mean radius being of order of one micron). Everything is left at rest until the thermodynamical equilibrium is reached. Then several decompression steps are applied rhythmically until a certain ambient pressure is reached, which approximates a constant decompression rate. After the final step, samples are very rapidly cooled, in order to quench bubbles in the magma. Thanks to microscopic observations, the number of bubbles is evaluated and theirs radii are measured so as to obtain a table with bubbles separated in classes of radius. An experimental series is defined by several experiments quenched at progressively lower final pressures under identical starting conditions and decompression rate. The nucleation step, however, cannot be reproduced exactly from an experiment to another. As a result, samples have slightly different initial bubble size distributions. These differences, although visible on the tabulated data, are smaller than the changes induced by coalescence and growth. Experimental conditions fix the values of T, α_0, η_{eff}, Σ, ρ_m, D, ΔP, P_i, C_i. The scaling value R_i is defined as the mean bubble radius over all the measured radii at initial time.

We first verify our expansion model by neglecting coalescence. We recall that the ambient pressure acts in this model as the inverse of time, so that when time varies from 0 to 1, ambient pressure varies from 1 to 0. We consider the following initial data, before scaling:

$$f_{ij}^0 \Delta v_i \Delta m_j = \delta_{20,20}$$

with $\delta_{I,J}$ a Dirac mass such that $\delta_{I,J} = 1$ if $i = 20$ and $j = 20$, zero otherwise. This function corresponds to a mono-disperse initial data, that is we consider a population of bubbles with all the same radius and mass. The physical initial conditions are the following: the porosity is $\alpha_0 = 7.79\%$, the diffusion coefficient is $D = 10^{-10}\ m^2\ s^{-1}$, the volatile concentration is $C_i = 4.21$, the ambient pressure $P_a(0) = 10^8\ Pa$, the surface tension is $\sigma = 0.1\ Jm^{-2}$, the magma density is $\rho_m = 2400\ kg\ m^{-3}$, the temperature is $T = 825\ ^oC$, the decompression rate is $\Delta P = 10^5\ Pa\ s^{-1}$, the mean radius is $R_m = 10^{-5}\ m$, the uniform radius step is $\Delta R = 0.5 \cdot 10^{-6} m$ and we choose $N = 250$ discretization points.

The two relaxation parameters, Θ_V and Θ_D, in equations (31)-(30) are related to the experimental data by:

$$\Theta_V = \frac{4\eta_{eff}\,\Delta P}{P_i^2}\ , \quad \Theta_D = \frac{\Delta P R_i^2}{D\,P_i}\ . \tag{37}$$

where the quantities indexed by i are computed from the initial values.

We note here that we assume that the temperature T, as well as the diffusion coefficient D, and the viscosity one, η_{eff}, are constant. This is of course not always the case as also shown in [11] and considered in [7], and generalization to variable temperature, viscosity and diffusion is possible, but goes beyond the aim of this article.

The validation is carried out by comparing the outputs of three different computations. The two firsts (edp and edo simpl) refer to the simplified mono-disperse model and the kinetic model. Both are based on the approximation of the flux term in the mass rate (19). A perfect match between these two models indicates that the implementation of the kinetic model is correct. The third computation (edo gen) refers to the original mono-disperse model, with the coupling with the advection-diffusion equation (11). It is used as a reference so as to assess the impact of the simplified flux.

In figure 3 we show the behavior of the solutions for four couples of the relaxation parameters, $(\Theta_V, \Theta_D) = (10^{-3}, 10)$, $(\Theta_V, \Theta_D) = (10^{-5}, 10)$, $(\Theta_V, \Theta_D) = (10^{-5}, 10^{-3})$ and $(\Theta_V, \Theta_D) = (10^{-1}, 10^{-1})$. The first two couples (top) correspond to two physical situations far from the chemical equilibrium, $\Theta_D \gg 0$, one of them being at the mechanical equilibrium (top-right), the smallest Θ_V, and the other one not (top-left). In both cases, the difference between the simplified mono-disperse model and the kinetic equation is negligible. The third model deviates from the two approximate models at low pressures. These results suggest that the kinetic model implementation is correct, but that the simplified flux introduces discrepancies. Considering that the values of the relaxation parameter Θ_D represent a worse-case scenario with respect to the modeling situations to which we apply our model, it appears that the flux approximation is acceptable.
The other two couples (bottom) correspond to the thermodynamical equilibrium with the smallest relaxation parameters values (bottom-left), and to a case neither at the mechanical, or at the chemical equilibrium (bottom-right). We note the very good agreement for the equilibrium case, which includes a radius jump at the beginning of the computation due to the initial data not at the thermodynamical equilibrium. The kinetic solution of the non-equilibrium case seems to better approximate the coupled system than the simplified system solution.

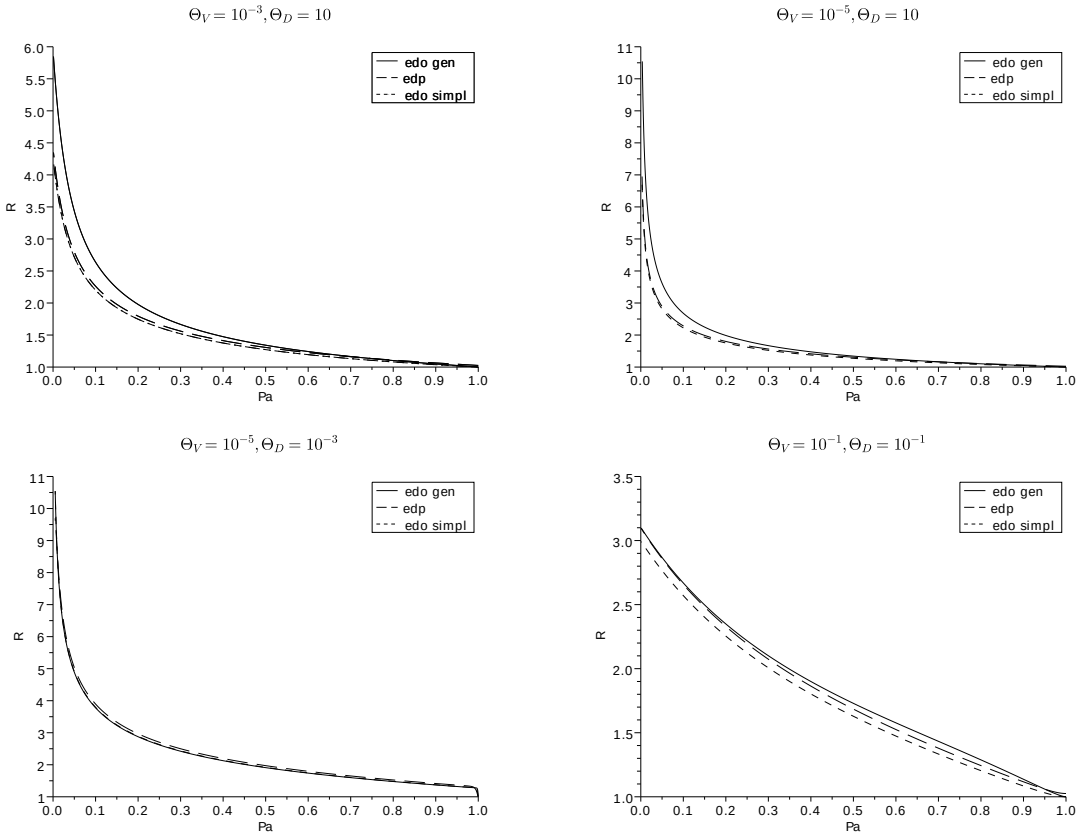

Figure 3: Comparison between the solution of the mono-disperse coupled system (edo gen), the simplified one (edo simpl) and the solution of the kinetic equation (edp).

We now compare the numerical solution of the kinetic model with the experimental data given in [1]. The initial condition corresponding to the data $ABG1$, reads in the kinetic framework:

$$f_{ij}^0 \Delta v_i \Delta m_j = \frac{1}{127} \sum_{k=18}^{34} D_k \delta_{k,k} \tag{38}$$
$$D = (1, 4, 7, 18, 17, 14, 19, 12, 11, 10, 4, 3, 1, 2, 1, 1, 1).$$

with $\delta_{I,J}$ Dirac masses such that $\delta_{I,J} = 1$ if $i = I$ and $j = J$, zero otherwise.

We compare in figure 4 the size distributions computed by our code (curves) and the data $PPE4$, $PPE1$, $PPE10$, and $PPE11$ (areas) of [1]. The physical values

are the following: the decompression rate is $\Delta P = 5 \cdot 10^5\ Pa\ s^{-1}$, the viscosity is assumed constant at $\eta_{eff} = 9 \cdot 10^5\ Pa\ s$, the temperature is $T = 825\ ^oC$, the surface tension is $\sigma = 0.1\ N\ m$, the magma density is $\rho_m = 2354\ kg\ m^{-3}$, the diffusion coefficient is $D = 6.95076 \cdot 10^{-12} m^2\ s^{-1}$. Initial values are from experiment $PPE4$: the volatile concentration is $C_i = 0.021756$, the porosity is $\alpha_0 = 51.2\%$, the ambient pressure is $P_a(0) = 40\ MPa$, and the scaling radius is $R_i = 111\ \mu m$. Experiments $PPE1$, $PPE10$, and $PPE11$ were quenched at 30, 28, and 24 MPa, which correspond to dimensionless times $t = 0.25, 0.3$, and 0.4, respectively. The initial size distribution from $PPE4$ was obtained by counting 127 bubbles, which were then sampled in regular intervals of 2.5 μm. Simulations kept that sampling interval with $N = 100$ discretization points. The other experimental distributions, however, were obtained by counting a very small number of bubbles because they became of a size comparable to the sample. This has two consequences. First, we found preferable to resample both the simulations results and the experimental data to intervals of 12.5 μm for comparison (see figure 4). Second, it precludes the comparison between experimental and simulated porosities. Coalescence led some large bubbles to connect with the sample outer surface, thereby leaving the sample and causing the porosity measure to be underestimated and unreliable. Sample $PPE1$, for instance, as a measured porosity of 30%, which is below the starting porosity of $PPE4$ (51.2%), and hence also below that predicted by the three simulations ($\sim 61\%$).

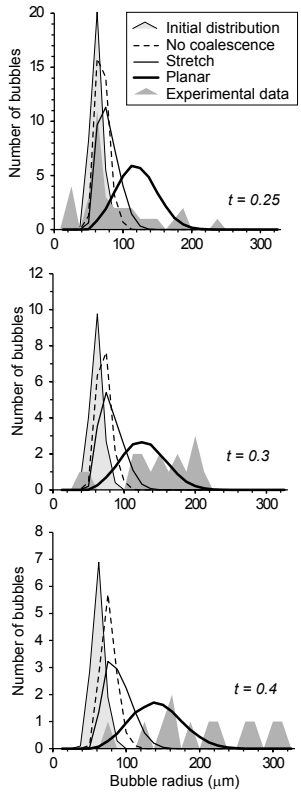

Figure 4: Comparison between numerical runs and experimental data from [1]. The initial distributions are shown in light gray and correspond to sample $PPE4$ and to the initial conditions of the runs. Experimental data are shown in dark gray areas. Dashed curves are runs with $H = 0$, thin solid curves are runs with $H = H_s$, and thick solid curves are runs with $H = H_p$. For each dimensionless time (0.25, 0.3, and 0.4), simulated distributions were scaled back to the number of bubbles counted in the respective experiment. The jagged appearance of the experimental distributions is due to the fact that intervals contain an integer number of bubbles. The presence of experimental bubbles smaller than the initial distribution at $t = 0.25$ can be explained by a smaller nucleation population for that sample rather than bubble breakup.

After a short while (around $t \sim 0.1$), the time steps became vanishingly small ($< 10^{-10}$), which caused prohibitively long calculation times (on the order of several months). These small time steps are due to numerical diffusion from bubble-bearing bins ($f^n \gg 0$) into near-zero bins (in practice between machine precision and 10^{-10}). A limiting condition so that $f^n \geq 10^{-10}$ was thus added at the end of each iteration.

This kept the time steps above 10^{-5} and the run times to less than an hour on an ordinary PC. We tested the accuracy loss by graphically superimposing the solutions with and without the limiting condition and found them to be negligible. A more accurate estimate is hindered by the fact that time steps are not identical between the runs. It can nevertheless be stated that the percent errors on the marginal with respect to the volume are of the same order as the percent in time differences (i.e. $10^{-6} - 10^{-7}$).

Three simulations are shown on figure 4. The first run has no coalescence ($H = 0$), in the second run coalescence occurs by planar film thinning ($H = H_p$), and in the third run coalescence occurs by stretching of inter-bubble films ($H = H_s$). It is apparent on figure 4 that planar coalescence is more effective than the stretching one because much larger bubbles are produced at all times. The match between planar coalescence and the experimental data is qualitatively the best, although it is clear that experimental distribution are based on too few bubbles to carry out a quantitative comparison. In the absence of more precise experimental data, it can be concluded that the implementation of kernels H based on different physical mechanisms yield distinct evolutions of the size distributions. Our kinetic model is thus a powerful tool that can help assessing how bubble coalescence occurs in magmas.

In Figure 5 we plot the 2D distribution function for the initial data (left) and the final time $T = 0.4$ (right) in the case of planar coalescence Q_p and for the previous set of experimental data. We note that the distribution function is concentrated on the equilibrium manifold defined by the chemical and mechanical equilibria.

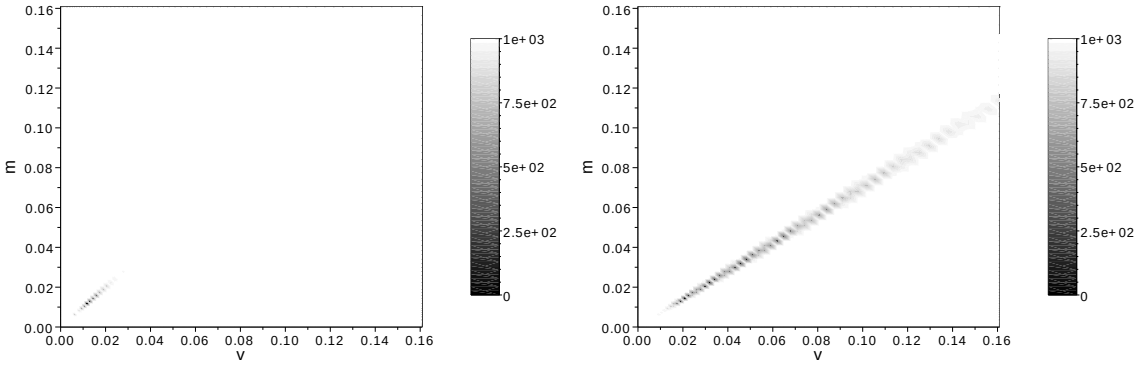

Figure 5: Bi-dimensional solution: left - initial data; right - time $T = 0.4$.

7 Conclusions

The growth of volatile bubbles in very viscous fluids has been widely described in the mono-disperse framework, which is based on the microscopic description of a single bubble.

Starting from the analysis of a mono-disperse bubble population done in [11] and [9], we build a kinetic model statistically describing the growth by decompression, exsolution and coalescence of a poly-disperse bubble population. The proposed model is homogeneous in space and the distribution function represents the probability to find a bubble of volume v and mass m at time t. The volume and mass growth rates are described in agreement with a simplification of the original microscopic model [11] that avoids the resolution of the diffusion of water in the melt. Coalescence is two-dimensional in the proposed model, its rate involving both volumes and masses of the coalescing bubbles, see [3]. Numerical simulations based on a semi-implicit numerical scheme show a good agreement for the coalescence-free case with those of the mono-dispersed model. When coalescence is introduced, numerical results show that coalescence kernels based on different physical mechanisms yields distinct evolutions of the size distributions. In the case presented, experiments underwent extensive coalescence, which yielded poorly defined distribution. This nevertheless allowed us to show a qualitative match of one out of three possible kernels. Our kinetic model is thus a powerful tool that can help assessing how bubble coalescence occurs in magmas.

Several simplifications have been done in order to write this model. For instance, the coupling with an advection-diffusion equation describing the behavior of the volatile concentration in the fluid has been simplified considering a mass growth rate converging to the chemical equilibrium for small values of the relaxation parameter Θ_D. Finally, bubbles coalescence has been assumed as instantaneous, that is the created bubble is instantaneously spherical. Of course, this is not real, and it is possible to see the formation of chains of bubbles during the decompression. This is a relevant factor for the modeling of bubbles growth in volcanoes, and need to be taken into account in future works. In fact, it is directly linked to the permeability and to the possibility for the volatile to exit the magma or to accumulate giving rise to an explosive eruption.

Finally, from a mathematical and modeling point of view, it may also be of interest to study the convergence of this kinetic model towards simplified ones. For instance in [9] we have deduced several limit situations when the relaxation param-

eters Θ_V and Θ_D converge to zero or infinity, simultaneously or not. Performing an asymptotic analysis on the proposed kinetic model should give simplified equations corresponding to the above limits cases leading to faster computational times.

References

[1] A. Burgisser and J.E. Gardner. Experimental constraints on degassing and permeability in volcanic conduit flow. *Bull. Volc.*, 67:42–56, 2005.

[2] J. A. Carrillo, L. Desvillettes, and K. Fellner. Exponential decay towards equilibrium for the inhomogeneous Aizenman-Bak model. *Comm. Math. Phys*, 278(2):433–451, 2008.

[3] J. M. Castro, A. Burgisser, I. Schipper, and S. Mancini. Mechanisms and dynamics of bubble coalescence in silicic magmas. *Bull. Volcan.*, 74(10):2339–2352, (2012).

[4] B. Chouet, P. Dawson, and M. Nakano. Dynamics of diffusive bubble growth and pressure recovery in a bubbly rhyolitic melt embedded in an elastic solid. *J. Geophys. Res.*, 111, 2006.

[5] M. Escobedo, P. Laurençot, and S. Mischler. On a kinetic equation for coalescing particles. *Comm. Math. Phys.*, 246(2):237–267, 2004.

[6] F. Filbet and P. Laurençot. Numerical simulation of the Smoluchowski equation. *SIAM J. Sci. Comput.*, 25:2004–2028, 2004.

[7] L. Forestier-Coste. *Croissance et coalescence de bulles dans les magmas : analyse mathématique et simulation numérique*. PhD thesis, Université d'Orléans, 2012. `http://tel.archives-ouvertes.fr/tel-00736634`.

[8] L. Forestier-Coste and S. Mancini. A finite volume preserving scheme on nonuniform meshes and for multidimensional coalescence. *SIAM J. Sci. Comp.*, 34(6):B840–B860, (2012).

[9] L. Forestier-Coste, S. Mancini, A. Burgisser, and F. James. Numerical resolution of a mono-disperse model of bubble growth in magmas. *Appl. Math. Mod.*, 36:5936–5951, 2012.

[10] R. Kumar, J. Kumar, and G. Warnecke. Numerical methods for solving two-dimensional aggregation population balance equations. *Chem. Eng. Sci.*, 35:999–1009, 2011.

[11] N.G. Lensky, O. Navon, and V. Lyakhovsky. Bubble growth during decompression of magma: experimental and theorical investigation. *J. Volc. Geoth. Res.*, 129:7–22, 2004.

[12] S. Lovejoy, H. Gaonac'h, and D. Schertzer. Bubble distributions and dynamics: The expansion-coalescence equation. *J. Geophys. Res.*, 109, 2004.

[13] V. Lyakhovsky, S. Hurwitz, and O. Navon. Bubble growth in rhyolitic melts: experimental and numerical investigation. *Bull. Volcanol.*, 58(1):19–32, 1996.

[14] A.A. Proussevitch, D.L. Sahagian, and A.T. Anderson. Dynamics of diffusive bubble growth in magma: isothermal case. *J. Geophys. Res.*, 98:22283–22307, 1993.

[15] S. Qamar and G. Warnecke. Numerical solution of population balance equations for nucleation growth and aggregation processes. *Comp. Chem. Eng.*, 31:1576–1589, 2007.

[16] S. Qamar and G. Warnecke. Solving population balance equations for two-component aggregation by a finite-volume scheme. *Chem. Eng. Sci.*, 62:679–693, 2007.

[17] S. Qamar, G. Warnecke, and M.P. Elsner. On the solution of population balances for nucleation, growth, aggregation and breakage processes. *Chem. Eng. Sci.*, 64:2088–2095, 2009.